American Journal of Materials Science and Application
2014; 2(5): 76-85
Published online October 20, 2014 (http://www.openscienceonline.com/journal/ajmsa)

Hyperelastic modelling and limit stress prediction of natural rubber/rubber seed oil (*Hevea brasiliensis*) modified kaolin composites

Chukwutoo Christopher Ihueze[1], Chinedum Ogonna Mgbemena[2]

[1]Department of Industrial Production Engineering, Nnamdi Azikiwe University, Awka, Nigeria
[2]Department of Mechanical Engineering, Federal University of Petroleum Resources, Effurun, Nigeria

Email address

mgbemena.ogonna@fupre.edu.ng (C. O. Mgbemena)

To cite this article

Chukwutoo Christopher Ihueze, Chinedum Ogonna Mgbemena. Hyperelastic Modelling and Limit Stress Prediction of Natural Rubber/Rubber Seed Oil (*Hevea brasiliensis*) Modified Kaolin Composites. *American Journal of Materials Science and Application.* Vol. 2, No. 5, 2014, pp. 76-85.

Abstract

This study deals on hyperelastic modeling and prediction of limit stresses of organo-kaolin filled natural rubber vulcanizates with the filler oleochemically derived from the complex intercalate of hydrazine hydrate and rubber seed oil (*Hevea brasiliensis*) modified kaolin for tyre side wall applications. The stress-strain data reports of Natural Rubber/Rubber Seed Oil modified kaolin (NR/RSO) obtained from uniaxial tests conducted were used to develop hyperelastic models by employing ANSYS 14.0 software. The Yeoh 3rd Order model was observed to give perfect fit for NR/RSO modified kaolin composites. The energy absorption capacities were evaluated on the functions derived from stress-strain data to establish the toughness of NR/Unmodified Kaolin and NR/RSO modified Kaolin. The NR/Unmodified kaolin composite has its approximate strain energy as 29.1147MJ/m^3 at 2phr while the NR/RSO kaolin composite has its approximate strain energy as 51.5899MJ/m^3 at 10phr. Plane stress analysis executed on ANSYS 14.0 gave limit stress distributions in terms of von-Mises stresses in the range 1.28897MPa-1.41134MPa. The maximum principal stress is found to be higher than the ultimate tensile strength of 1.335938MPa hence the material is safely specified with load range of von-Mises 1.28897MPa-1.335938MPa. Atomic Force Microscopy conducted on the respective natural composites further validated micromechanically the reason for optimum results obtained for NR/RSO modified kaolin composites.

Keywords

Hyperelastic Behaviour, Energy Absorption Capacity, Strain Energy, Von-Mises Stress, AFM

1. Introduction

Natural Rubber is an essential commodity in industry and daily life following the discovery of the vulcanization technique by Charles Goodyear and Thomas Hancook in the years 1839-1844. This discovery led to the upsurge in industrial applications of Natural Rubber and its derivatives. Natural Rubber composites have numerous industrial application areas such as automobiles, aerospace, industrial machinery and packaging. In automobiles, Natural rubbers composites are applied in vehicle tire sidewalls and tubes, as door seals and engine seals. In aerospace, they are used in fuel systems. In other engineering fields, they have been applied in conveyor belts, meteorological balloons and bearings of foundations.

Material scientists, Design engineers and Polymer chemists are in continuous research of functional materials from elastomers that will be applied in service which entails that selection of materials for engineering design is of major significance for service delivery. Failure prediction for isotropic material subjected to uniaxial stress is performed by the design engineer to ensure that applied uniaxial stress does not exceed the ultimate strength of the material as specified in some material data sheet. However, some serving materials are subjected to multi-axial stress states which require more robust techniques to predict failure. Crawford

(1998) reported the various failure theories on maximum stress criterion, maximum strain criterion and Tsai-Hill criterion as appropriate for predicting failure of composite materials. Ihueze et al. (2013) and Ihueze et al. (2014) applied distortion energy theory (DET) implemented with ANSYS software to predict failure of plantain composites subjected to multi-axial stress state and limiting stresses of Natural Rubber/Tea Seed Oil modified kaolin composites designed and applied on automobile tire sidewalls.

Recent studies conducted by several researchers indicate that prediction of the onset of failure is more significant than the knowledge of the ultimate strength of material. Therefore to predict the limit stresses of a material; a thorough knowledge of the related orthogonal stresses, principal stresses and shear stresses of the multi-axial stressed material as manifested in von Mises stress theory and mastery of the finite element model (FEM) are required to solve the material model which represents the characteristic material properties and external effects (Sadek and Olson, 2014; Gross and Ravi-Chandar, 2014; Mohotti et al, 2014).

Theoretical stress–strain relations that match experimental results for hyperelastic materials have been developed by various researchers (Miehe et al., 2004; Boyce and Arruda, 2000; Charlton and Yang, 1994). Mooney (1940) suggested a phenomenological model with two parameters based on the assumptions of a linear relation between the stress and strain during simple shear deformation. Treloar (1958) developed the neo-Hookean material model which is a special case of the Mooney model that is based on the statistical theory with only one material parameter. The Mooney and neo-Hookean strain energy function have played an important role in the development of the nonlinear hyperelastic theory and its applications (Ogden, 1984, 2001).

Rivlin (1948a, 1948b, 1949) obtained a general expression of the strain energy function expressed in terms of strain invariants from a modified Mooney model. Yeoh (1993) published one of the most successful hyperelastic models in the form of a third-order polynomial of the first invariant of the right Cauchy–Green tensor. Gent (1996) proposed a high-order polynomial model with the form of a natural logarithm of the first invariant. In 1972, Ogden (1972a, 1972b) proposed a strain energy function expressed in terms of principal stretches, which is a very general tool for describing hyperelastic material. An excellent agreement has been obtained between Ogden's formula and Treloar's experimental data for extensions of unfilled natural rubber up to 700% (Ogden, 1972a, 1972b). However, the parameter identification is complicated because of the purely phenomenological character of the Ogden strain energy function.

In this present study, the experimental results of Mgbemena (2014) will be employed to perform hyperelastic modelling of Natural Rubber/Rubber Seed Oil modified composites (NR/RSO); analyze the stress strain response of the composites using ANSYS Workbench 14.0 and predict failure from the limit stress distribution of the maximum principal stresses and von Mises stresses at different positions of the material.

2. Methodology

2.1. Materials and Data

The materials employed in this study and the method of preparation of rubber seed oil modified kaolin are as contained in the previous work published by the following authors (Mgbemena et al., 2013a; Mgbemena et al., 2013b; Rugmini and Menon, 2008).

2.1.1. Preparation of Rubber Vulcanizates

Replicated samples of Natural Rubber/Rubber seed oil modified kaolin composites were compounded by melt blending as shown in Table 1. The melt blending process demands the dispersal and exfoliation of an organoclay into an elastomer while being masticated by high shear forces from an open two-roll mill. The rubbers are blended with accelerants, activators, kaolin, softeners and Sulphur. The blend mixtures were plasticized for about 12–15 min and thin-passed several times at 90°C. Rubber vulcanizates sheets of dimension 90 mm × 90 mm × 1.5 mm were prepared by compression molding at a temperature of 140°C for 10 min on an electrically heated, semi-automatic hydraulic press (MODEL INDUDYOG DS-SD-HMP/25) at 400 Pa and curing takes place at the same temperature and pressure.

Table 1. *Composition of the rubber composites*

Ingredients (phr)	UMK	RMK
Natural Rubber	100	100
Zinc Oxide	5	5
Stearic Acid	2	2
URK	2,6,10	-
MRK	-	2,6,10
MBT	2	2
Sulphur	2	2

UMK is the unmodified Kaolin; RMK is the Rubber Seed Oil modified Kaolin; MBT is Mercapto Benzothiazole.

2.2. Hyperelastic Modeling and Curve Fitting of Stress-Strain Data

Hyperelastic models are a feature in most commercial Finite Element Analysis (FEA) software. The uniaxial test data was used to obtain the coefficients of the strain energy function and the hyperelastic models. The material parameters of the various composites optimized in this work were obtained by the fitting of the strain energy function to stress-strain data using ANSYS Workbench 14.0. The optimization process was used in the ANSYS software to minimize the error with respect to the model's parameter.

2.3. Estimation of Energy Absorption Capacities of the Composites

The energy absorption capacities of the optimum setting of the composites were estimated using trapezoidal rule by computing the area under the stress-strain curve. Newton-Cotes integration formulas (trapezoidal rule, Simpson's rule

and Richardson's extrapolation (Romberg integration)) are possible integration schemes to evaluate the area under the curve.

2.4. Failure Analysis

The octahedral shear stress theory (distortion energy or Henky-von Mises) was used as the preferred method for predicting the onset of yielding, for materials exhibiting equal strengths in tension and compression (Shigley and Mischke, 1986) and is classically expressed as

$$\tau_0 = \frac{1}{3}[(\sigma_1 - \sigma_2)^2 + (\sigma_2 - \sigma_3)^2 + (\sigma_3 - \sigma_1)^2]^{1/2} \quad (1)$$

Equation (1) can be re-expressed in terms of orthogonal component stresses as

$$\tau_0 = \frac{1}{3}\left[\left(\sigma_x - \sigma_y\right)^2 + \left(\sigma_y - \sigma_z\right)^2 + (\sigma_z - \sigma_x)^2 + 6\tau xy2 + \tau yz2 + \tau zx212\right. \quad (2)$$

The limiting value of the octahedral shear stress is that which occurs during uniaxial tension at the onset of yield and is expressed as

$$\tau_0 = \frac{\sqrt{2}\, S_y}{3} \quad (3)$$

Expressing (3) in terms of the principal stresses and a design factor, we obtain

$$\frac{S_y}{n} = \frac{3}{\sqrt{2}}[\tau_0]\text{lim} = \frac{1}{\sqrt{2}}[(\sigma_1 - \sigma_2)^2 + (\sigma_2 - \sigma_3)^2 + \sigma 3 - \sigma 1212 = \sigma' \quad (4)$$

The term σ' is called the von Mises stress. It is the uniaxial tensile stress that induces the same octahedral shear (or distortion energy) in the uniaxial tension test as does the triaxial stress state in the actual part.

Where,

$\sigma_1, \sigma_2, \sigma_3$= are the ordered principal stresses,

$\sigma_{x,\ \sigma_y,\ \sigma_z}$ = are the orthogonal stresses in x, y and z-directions respectively,

$\tau_{xy}, \tau_{yz,}\ \tau_{zx}$ = orthogonal shear stresses,

S_y = uniaxial yield stress,

σ' = von Mises stress,

n =design safety factor

Most FE solvers used for failure analysis implements for linear elastic isotropic materials, the plane stress material model expressed as

$$\begin{bmatrix}\sigma_x \\ \sigma_y \\ \tau_{xy}\end{bmatrix} = \frac{E}{1-\mu^2}\begin{bmatrix}1 & \mu & 0 \\ \mu & 1 & 0 \\ 0 & 0 & (1-\mu)/2\end{bmatrix}\begin{bmatrix}\varepsilon_x \\ \varepsilon_y \\ \gamma_{ZZ}\end{bmatrix} \quad (5)$$

This entails that with the material properties of elastic modulus E and Poisson's ratio μ the orthogonal stresses and principal stresses can be estimated in a finite element solver system. Also implemented is the strain-displacement relationships expressed as

$$\varepsilon_x = \frac{\partial u}{\partial x}, \varepsilon_y = \frac{\partial v}{\partial y}, \gamma_{xy} = \frac{\partial u}{\partial y} + \frac{\partial v}{\partial x} \quad (6)$$

The robustness of this analysis requires the evaluation of yield stresses obtained as von-Mises stresses, orthogonal stresses and etc. In this work ANSYS 14.0 was used to solve for plane stresses and subsequently the yield stress distribution.

2.5. Atomic Force Microscopy (AFM) of Natural Rubber Composites

In order to obtain a very smooth sample surface for AFM imaging, the samples were first cooled in air by cryomicrotoming process and then sliced to the required sample sizes. The measurements were carried out in air at an ambient temperature (25^{o}C) using tapping mode probe with constant amplitude. The scanning was done at different positions for each sample and the best images recorded. The measurements for the samples were done on the same size of scan area for comparison purposes. AFM was performed with a view to ascertain the correlation of the morphological property of the composites with parameters characterizing the linear isotropic elastic behaviour of the rubber vulcanizates. NR/Unmodified kaolin composites at 10phr and NR/Rubber Seed Oil modified kaolin composites at10phr respectively were analyzed.

2.5.1. Roughness Analysis

The changes in surface topography could be determined quantitatively by the root mean square (RMS) roughness calculation (Rq). This is applied when the surfaces show a degree of randomness. The roughness calculation is based on finding a median surface level for the image and then evaluating the standard deviation within the image. Since the roughness analysis is based on the vertical axis, i.e., the z-axis, the topographic height images were used in the present investigations. Root mean square average of height deviations taken from the mean data plane was expressed by (Maiti and Bhowmick, 2006) as:

$$R_q = \sqrt{\frac{\sum(Z_i)^2}{n}} \quad (7)$$

where

Z_i= current Z value

$n =$ Number of points on the image

R_a= the mean roughness (this is the arithmetic average of the absolute values of the surface height deviations measured from the mean plane:

$$R_a = \frac{1}{n}\sum_{j=1}^{n}\left|Z_j\right| \quad (8)$$

2.5.2. Particle Size and Filler Distribution

In the tapping mode, the measurement of the difference between the phase angle of the excitation signal and the phase angle of the cantilever response is used to map compositional variations such as stiffness, hardness and viscoelasticity on the sample surface.

The phase image can provide a stiffness variation in the

sample, which is expressed by the following equation:

$$\Delta\varphi_0 \approx \langle S\rangle\left(\frac{Q}{k}\right) = \varepsilon\langle a\rangle E^*\left(\frac{Q}{k}\right) \quad (9)$$

where

$\Delta\varphi_0$ = the phase angle shift between free and interacting cantilevers,

S = the stiffness of the material,

Q = The quality factor, which is a measure of viscous damping of the cantilever,

ε = Constant

a = the radius of the contact area between tip and the surface,

E^*= the effective modulus of the material,

$\langle S\rangle$ and $\langle a\rangle$ are time-averaged values of the stiffness S, and contact radius a, over one cycle of oscillation. Hence, a stiffer region will correspond to a greater value of $E^*$and $\Delta\varphi_0$.

3. Results and Discussions

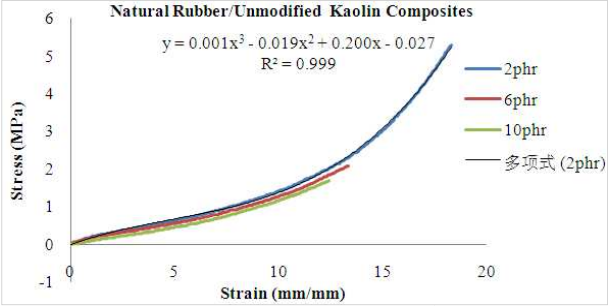

Figure 1. *Natural Rubber/Unmodified Kaolin Composites*

Figures 1 and 2 present the uniaxial tests results of unmodified and modified natural rubber composites. Both figures show hyperelastic nature of rubber composites as the recorded maximum strain at failures exceeded 500%. Figure 1 shows that at 2phr the unmodified kaolin natural rubber composite is more hyperelastic. While figure 2 shows that RSO modified kaolin rubber composite is more hyperelastic at 10phr.

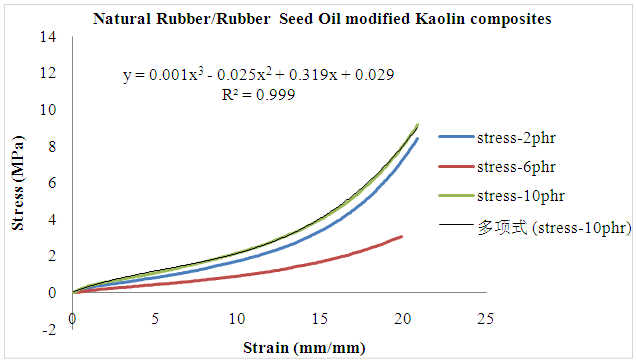

Figure 2. *Natural Rubber/Rubber Seed Oil modified Kaolin Composites*

Figure 3 is a depiction of the result of modeling the stress-strain response data of figure 2 of tensile test results of NR/RSO modified kaolin composites in ANSYS 14.0 Workbench choosing the Yeoh curve fitting function model. Table 2 is an exhibition of the Yeoh model parameters as evaluated with ANSYS FE work bench 14.0. The figure 3 actually shows that the strain energy density function of the material can be represented with the Yeoh 3rd order model so that by applying data of table 2 to the Yeoh model, the model representing the strain energy function of NR/RSO modified kaolin composites can be expressed as

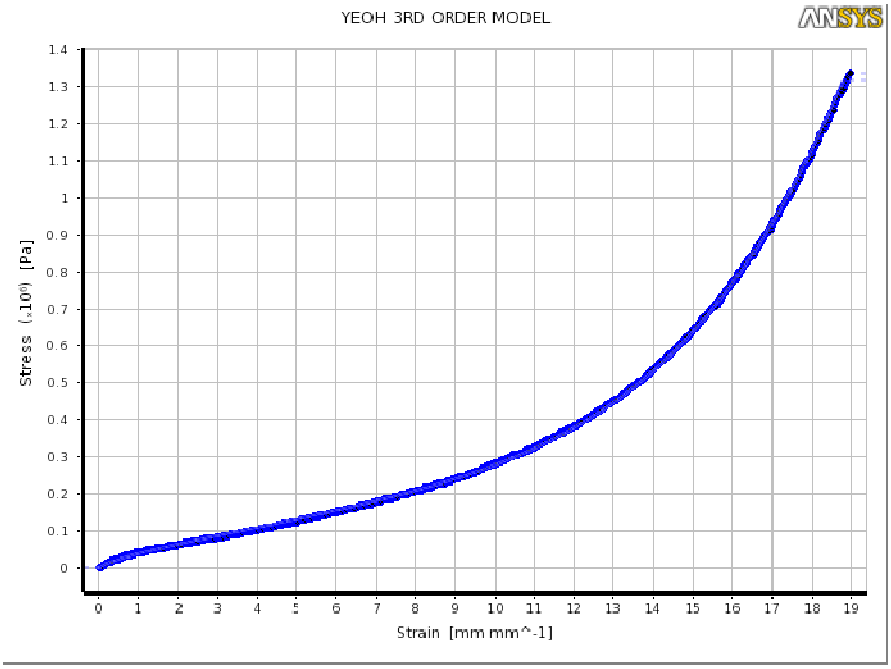

Figure 3. *Yeoh 3rd order model for NR/RSO kaolin at 10phr*

Table 2. *Computed Parameters for Yeoh 3rd order parameter model for NR/RSO kaolin at 10phr*

Coefficient Name	Calculated Value
Incompressibility Parameter D1	0 Pa^{-1}
Incompressibility Parameter D2	0 Pa^{-1}
Incompressibility Parameter D3	0 Pa^{-1}
Material parameter C10	1.1702E+05 Pa
Material parameter C20	-32.469 Pa
Material parameter C30	0.57028 Pa
Residual	1.3949

$$W = 117020(I_1 - 3)^1 - 32.469(I_1 - 3)^2 + 0.57028(I_1 - 3)^3 \quad (10)$$

or

$$W = 351367.61856 + 117230.21156I - 37.60152I^2 + 0.57028I^3$$

Newton-Cotes integration formulas (trapezoidal rule, Simpson's rule and Richardson's extrapolation (Romberg integration)) are possible integration schemes to evaluate the area under the curve. The trapezoidal rule for unequal segments (varying step size) is expressed in Chapara and Canale (1998) as:

$$I = h_1 \frac{f(x_0)+f(x_1)}{2} + h_2 \frac{f(x_1)+f(x_2)}{2} + \cdots + h_n \frac{f(x_{n-1})+f(x_n)}{2} \quad (11)$$

Data of figures 1 and 2 were used to generate data for tables 3 and 4 respectively and applied to equation (11) to implement trapezoidal rule for evaluation of energy absorbed.

Table 3. *Data for application of trapezoidal rule to unequal segments of function (f(x)) of NR/Unmodified kaolin composites at 2phr:*

I	x	h	$F(x_i)$	n	$h_n \frac{f(x_{n-1})+f(x_n)}{2}$
0	0.02		0.01		
1	0.54	0.52	0.10	1	0.0286
2	2.06	1.52	0.31	2	0.3116
3	2.88	0.82	0.39	3	0.2870
4	3.90	1.02	0.49	4	0.4488
5	5.54	1.64	0.68	5	0.9594
6	6.26	0.72	0.78	6	0.5256
7	7.78	1.52	1.10	7	1.4288
8	8.54	0.76	1.12	8	0.8512
9	9.68	1.14	1.33	9	1.3965
10	10.82	1.14	1.58	10	1.6587
11	12.24	1.42	1.95	11	2.5063
12	13.44	1.20	2.32	12	2.5620
13	14.58	1.14	2.80	13	2.9184
14	15.68	1.10	3.38	14	3.3990
15	16.60	0.92	3.95	15	3.3718
16	18.02	1.42	5.05	16	6.4610
				I=TOTAL	29.1147

The area under the stress strain curve response of NR/unmodified composite is then estimated as 29.1147MJ/m^3.

Table 4. *Data for application of trapezoidal rule to unequal segments of function (f(x)) of NR/RSO kaolin composites at 10phr:*

I	x	h	$F(x_i)$	n	$h_n \frac{f(x_{n-1})+f(x_n)}{2}$
0	0.04		0.02		
1	1.13	0.90	0.41	1	0.1935
2	2.08	0.95	0.59	2	0.4750
3	4.53	2.45	1.00	3	1.94775
4	4.75	0.22	1.05	4	0.2255
5	6.18	1.43	1.32	5	1.69455
6	7.75	1.57	1.66	6	2.3393
7	9.15	1.40	1.97	7	2.541
8	10.65	1.50	2.37	8	3.255
9	12.08	1.43	2.83	9	3.718
10	13.98	1.90	3.52	10	6.0325
11	15.45	1.47	4.29	11	5.74035
12	16.93	1.48	5.20	12	7.0226
13	18.90	1.97	6.88	13	11.8988
14	19.55	0.65	7.58	14	4.6995
				I=TOTAL	51.58985

The area under the stress strain curve response of NR/unmodified composite is then estimated as 51.58985MJ/m^3.

Figure 4 shows the meshing of the composite investigated with constraint applied. Figures 5-10 present the elastic stresses distribution associated with the application of NR/RSO Modified kaolin evaluated with ANSYS 14.0 finite element software using experimentally derived elastic constants (elastic modulus and Poisson's ratio) and material density and assumption of linear elastic-isotropic material model to implement the plane stress, stress -strain model expressed in equations (1-6). von-Mises stresses were evaluated to be in the range 1.28897MPa to 1.41134MPa while the shear stresses are within the range -0.030443 to -0.030443MPa and the orthogonal stresses in x and y are -0.395922MPa to -0.797932MPa and 1.04344MPa to 1.62843MPa respectively.

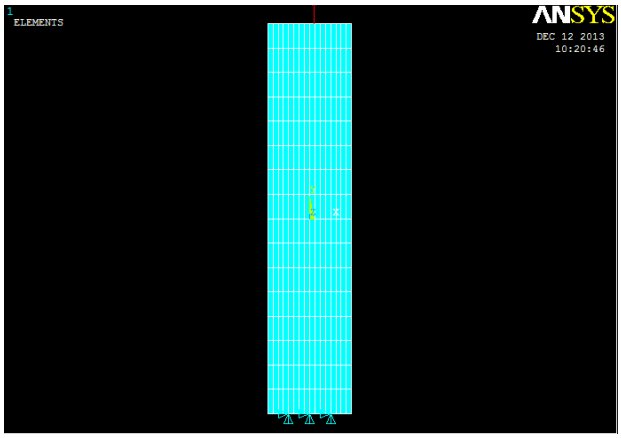

Figure 4. *Meshing of NR/Rubber Seed Oil modified kaolin at10phr with constraint applied*

Figures 11-13 compares stresses distribution of natural rubber/unmodified kaolin composites at 10phr with natural

rubber RSO modified kaolin composites to establish that the modification of kaolin increases the strength of natural rubber. The von-Mises stresses values of figure 13 of NR/RSO kaolin composite are more than that of NR/unmodified kaolin composite of figure 13.

The situation where the applied orthogonal and principal stresses are higher than the ultimate strength of material is unacceptable so that design engineer must apply load based on von Mises stresses not exceeding the ultimate strength of material. This situation is pronounced in figures 6, 8 and 10 where the values of the applied local stresses are more than the ultimate strength of material with value 1.335938MPa.

Table 5 gives comprehensive results of the stresses associated with plane stress analysis with ANSYS 14.0 describing the need to predict failure stress based on the principal stresses and the yield stresses. When any of the local stresses is greater than the specified material ultimate strength prediction is recommended to be based on the distortion energy theory (DET) or von Mises criteria or on the maximum shear stress theory (MSST) also known as known as Tresca yield criterion which states that a part subjected to any combination of loads will fail (by yielding or fracturing whenever the maximum shear stress exceeds a critical value.

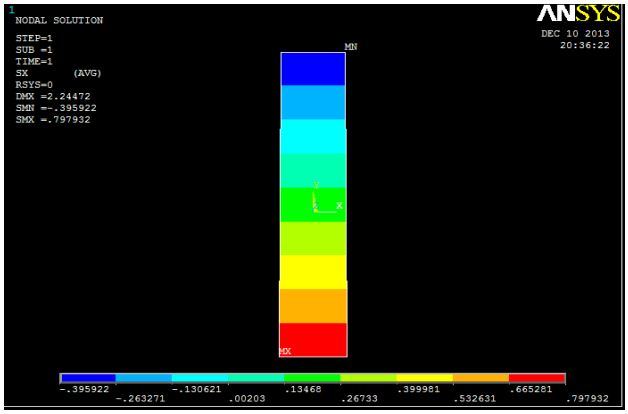

Figure 5. *ANSYS 14.0 Contour plot of distribution of X-component of stress for NR/RSO kaolin at10phr*

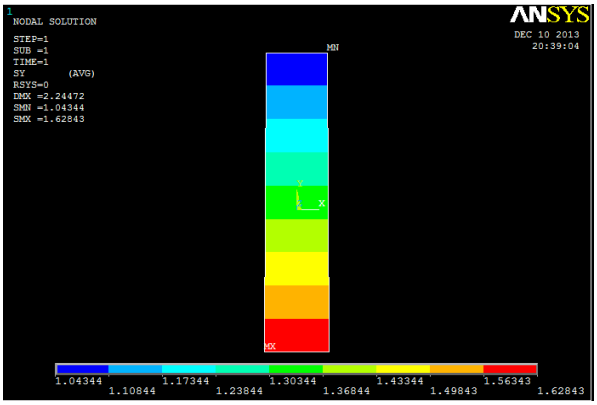

Figure 6. *ANSYS 14.0 Contour plot of distribution of Y-component of stress for NR/RSO kaolin at 10phr*

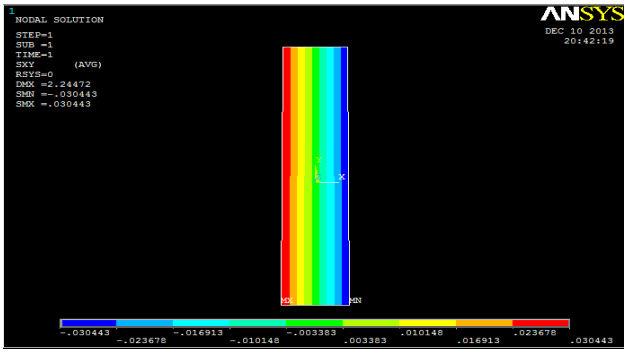

Figure 7. *ANSYS 14.0 Contour plot of distribution of XY Shear stress for NR/RSO kaolin at10phr*

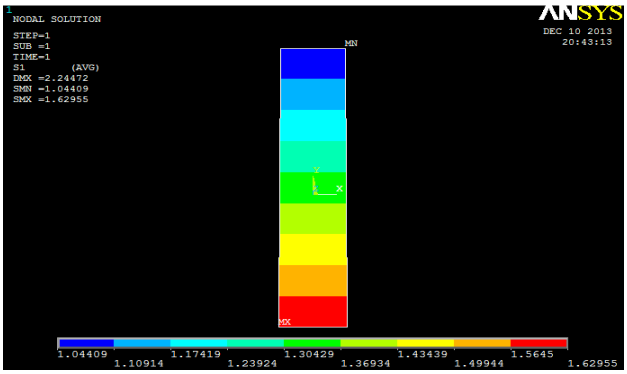

Figure 8. *ANSYS 14.0 Contour plot of distribution of maximum Principal Stresses for NR/RSO kaolin at 10phr*

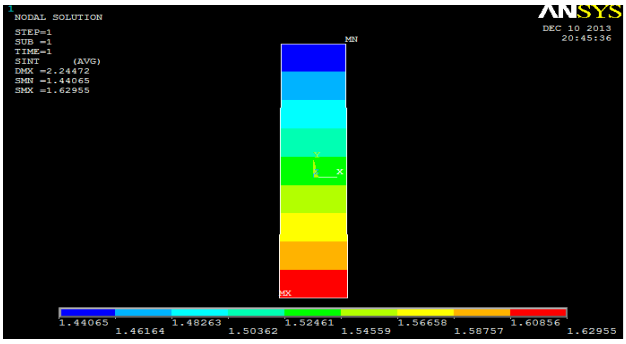

Figure 9. *ANSYS 14.0 Contour plot of distribution of stress intensity for NR/RSO kaolin at 10phr*

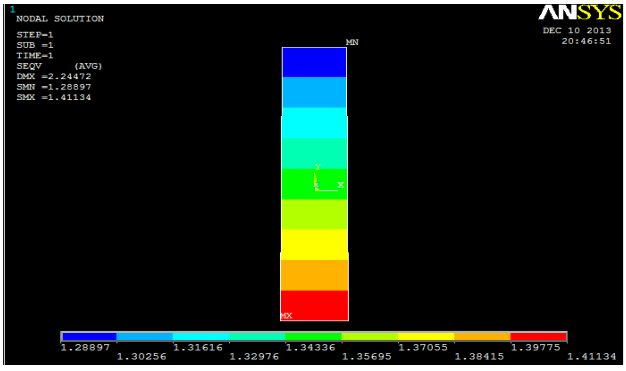

Figure 10. *ANSYS 14.0 Contour plot of distribution of Von Mises Stress for NR/RSO kaolin at 10phr*

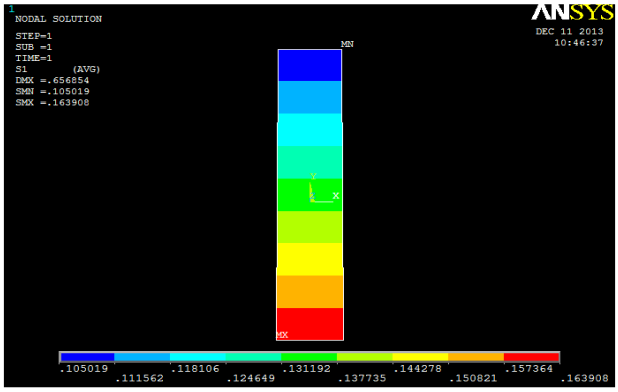

Figure 11. *ANSYS 14.0 Contour plot of distribution of maximum Principal Stresses for NR/Unmodified kaolin at10phr*

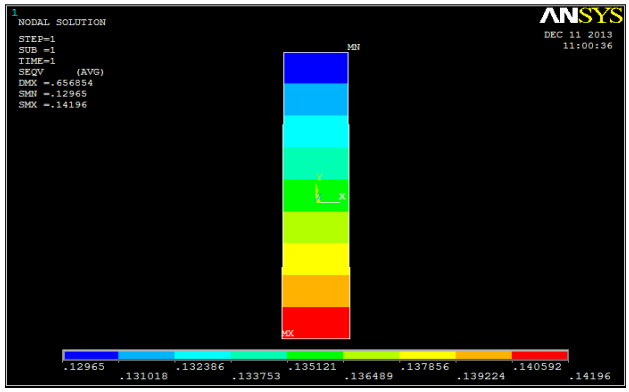

Figure 13. *ANSYS 14.0 Contour plot of distribution of Von Mises stress for NR/Unmodified kaolin at 10phr*

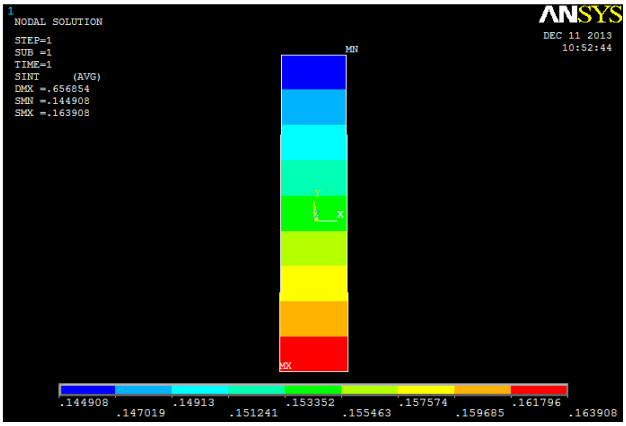

Figure 12. *ANSYS 14.0 Contour plot of distribution of stress intensity for NR/Unmodified kaolin at 10phr*

Table 5. *ANSYS 14.0 predicted failure stresses compared with ultimate stress of material*

Properties	NR/UMK/10phr		NR/RSOK/10phr	
	Min	Max	min	max
x-stress (MPa)	-0.039824	0.066917	-0.395922	0.797932
y-stress(MPa)	0.104955	0.157258	1.04344	1.62843
xy-stress(MPa)	-0.003062	0.002382	-0.030443	0.023678
1st principal stress(MPa)	0.105019	0.157364	1.04409	1.62955
2nd principal stress(MPa)	0	0.071242	0	0.708282
3rd principal stress(MPa)	-0.039888	-0.004432	-0.396565	-0.044063
Von Mises	0.12965	0.140592	1.28897	1.41134
Poisson's ratio	0.49		0.49	
Modulus of elasticity			0.02211	
Density				
Shear modulus				
Ultimate strength(MPa)	0.134375		1.335938	

4. Validation of Results

The results obtained from this study indicate that there are differences in the limit stresses obtained for NR/Unmodified kaolin and NR/Rubber Seed Oil modified kaolin composites. This observed differences can be explained from the results obtained from Atomic force microscopy of the composites at same filler concentration of 10phr. The phase images of the kaolin filled samples exhibit three shade differences: dark grey for the rubber matrix, grey for the rubber matrix near kaolin particles (interface region) and white for the kaolin particles. Table 6 and 7 shows the quantitative parameters obtained from AFM for the various composites and figures 14-17 shows the phase and 3D images of the composites investigated. The phase and 3D images for NR/Unmodified kaolin composites as depicted in figures 14 and 15 clearly shows that there the fillers were not well dispersed due to agglomeration of particles while compounding the composites as attributed to incompatibility of the filler-rubber surfaces. The phase image of Figures 16 for NR/RSO modified kaolin composite clearly show that the kaolin particles are well distributed over the rubber matrix. The 3D images for the NR/RSO modified kaolin composites in figure 17 further revealed the dispersion

of the fillers on the rubber matrix as indicated by the white coloured peaks. The various quantitative parameters obtained from the tapping mode AFM of the two samples clearly shows that NR/RSO modified kaolin composites has better parameters over NR/Unmodified kaolin composites with respect to the parametric values obtained for average roughness, R_a, Root mean square, R_q, Surface skewness, R_{sk} as shown in table 6 and 7.

Table 6. *Quantitative parameters from NR/Unmodified kaolin composites at 10phr*

Amount of sampling	65536
Max	1574.23 nm
Min	0 nm
Peak-to-peak, Sy	1574.23 nm
Ten point height, Sz	758.132 nm
Average	785.958 nm
Average Roughness,R_a	137.968 nm
Second moment	805.771
Root Mean Square, R_q	177.588 nm
Surface skewness, R_{sk}	-0.542907
Coefficient of kurtosis, Rka	0.605883
Entropy	13.4274
Redundance	-0.264408

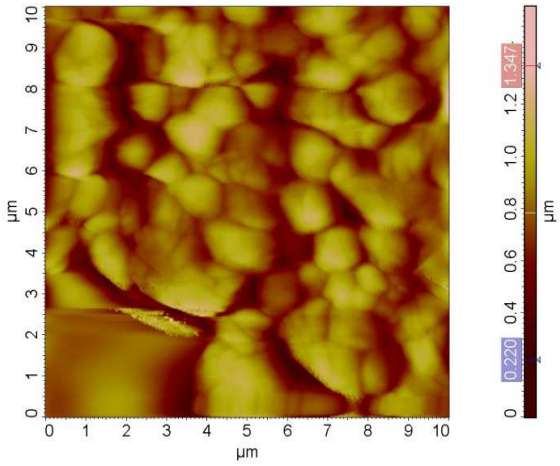

Figure 14. *Phase image of NR/Unmodified kaolin at 10phr*

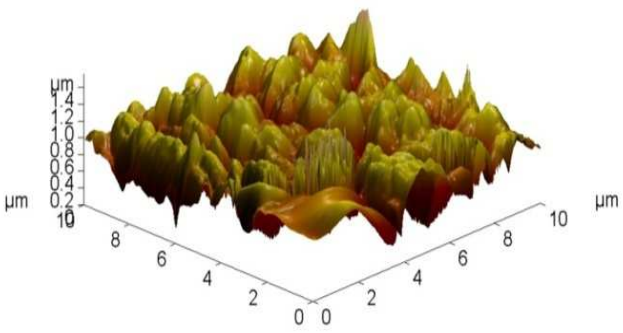

Figure 15. *3D images of the NR/Unmodified kaolin at 10phr*

Table 7. *Quantitative parameters from NR/RSO-modified kaolin composites at 10phr*

Amount of sampling	65536
Max	1440.09 nm
Min	0 nm
Peak-to-peak, Sy	1440.09 nm
Ten point height, Sz	723.568 nm
Average	888.874 nm
Average Roughness, R_a	153.669 nm
Second moment	910.702
Root Mean Square, R_q	198.187 nm
Surface skewness, Rsk	-0.661979
Coefficient of kurtosis, Ska	0.676284
Entropy	13.5505
Redundance	-0.291638

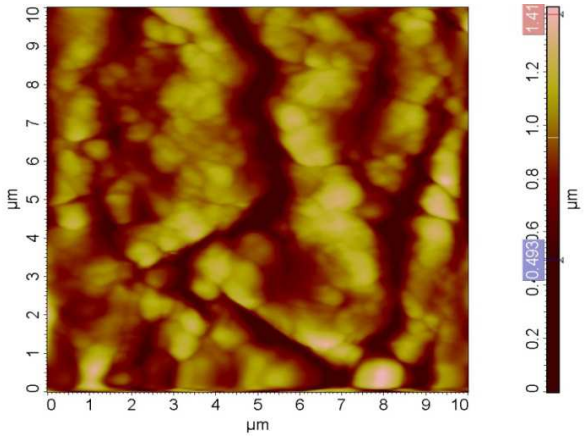

Figure 16. *Phase image of NR/RSO-modified kaolin at 10phr*

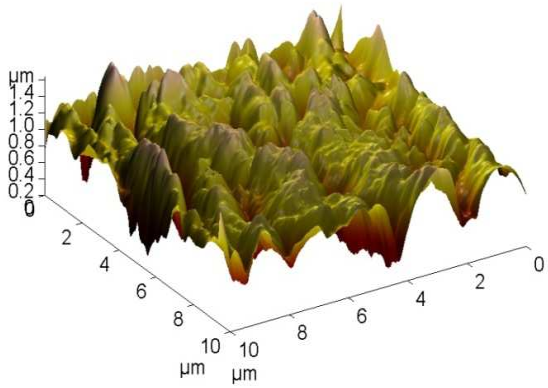

Figure 17. *3D images of the NR/RSO-modified kaolin at 10phr*

5. Conclusions

The following conclusions were drawn from this study:

1. The Stress– Strain results of NR/Unmodified kaolin composites are hyperelastic at 2hpr-10phr but NR/RSO modified kaolin composites are more hyperelastic at 2hpr-10phr.
2. The Yeoh 3rd order model fit was used to represent the value of the energy density function of NR/RSO modified kaolin composite.
3. The NR/Unmodified kaolin composite has its approximate strain energy as 29.1147MJ/m^3 at 2phr

while the NR/RSO kaolin composite has its approximate strain energy as 51.58985MJ/m^3.

4. Von-Mises stresses were evaluated to be in the range 1.20097MPa-1.41134MPa.
5. The maximum principal stress is found to be higher than the ultimate tensile strength of 1.335938MPa hence the material is safely specified with load range of von Mises, 1.20097MPa-1.335938MPa.
6. AFM is a veritable tool to validate linear isotropic elastic behaviour of the rubber vulcanizates and predicting the material with optimum characteristics.
7. The phase images of AFM as employed in this study for natural rubber composites can expose various heterogeneities and surface irregularities in the dissipation of mechanical energy on the polymer surface.
8. Quantitative parameters such as average roughness, R_a , Root mean square, R_q, Surface skewness, R_{sk} obtained from tapping mode AFM can be used in micromechanical failure analysis of composites as the values are in nanoscale.
9. Organomodification of kaolin with rubber seed oil (RSO) increases the strength of natural rubber composites.

References

[1] Arruda, E.M. & Boyce, M.C., (1993). A three-dimensional constitutive model for the large stretch behaviour of rubber elastic materials.Journal of the Mechanics and Physics of Solids 41, 389–412.

[2] Steinmann, P., Hossain, M. & Possart, G.,(2012). Hyperelastic models for rubber-like materials: consistent tangent operators and suitability for Treloar's data.*Arch ApplMech*, pp.1-35, DOI 10.1007/s00419-012-0610-z

[3] Charlton, D.J. & Yang, J. (1994). A review of methods to characterize rubber elastic behaviour for use in finite element analysis. Rubber Chemistry and Technology 67, 481–503.

[4] Miehe, C., Goktepe, S. & Lulei, F., (2004). A micro-macro approach to rubber-like materials—Part I: The non-affine micro-sphere model of rubber elasticity. Journal of the Mechanics and Physics of Solids 52, 2617–2660.

[5] Mooney, M.A., (1940). A theory of large elastic deformation. Journal of Applied Physics 11, 582–592.

[6] Ogden, R.W., (1972a). Large deformation isotropic elasticity—on the correlation of theory and experiment for the incompressible rubber-like solids. Proceedings of the Royal Society of London A 326, 565–584.

[7] Ogden, R.W., (1972b). Large deformation isotropic elasticity—on the correlation of theory and experiment for the compressible rubber-like solids. Proceedings of the Royal Society of London A 328, 567–583.

[8] Ogden, R.W., (1984). Non-linear elastic deformation. Dover Publications, Inc., Mineola, New York.

[9] Ogden, R.W. (2001). Nonlinear Elasticity. Cambridge University Press, Cambridge.

[10] Ogden, R.W. & Roxburgh, D.G. (1999). A pseudo-elastic model for the Mullins effect in filled rubber. Philosophical Transactions of the Royal Society of London A 455, 2861–2877.

[11] Rivlin, R.S. (1948a). Large elastic deformations of isotropic materials I. Fundamental concepts. Philosophical Transitions of the Royal Society of London A 240, 459–490.

[12] Rivlin, R.S. (1948b). Large elastic deformations of isotropic materials IV.Further developments of the general theory. Philosophical Transitions of the Royal Society of London A 241, 379–397.

[13] Rivlin, R.S. (1949). A note on the torsion of incompressible highly-elastic cylinder.Proceedings of the Cambridge Philosophical Society, 45, 485.

[14] Treloar, L.R.G. (1946). The elasticity of a network of long-chain molecules. Transactions of Faraday Society 42, 83–94.

[15] Treloar, L.R.G. (1958). The Physics of Rubber Elasticity, second ed. Oxford University Press, Glasgow.

[16] Chapra, S.C. & Canale, R.P. (2006). Numerical Methods for Engineers, fifth ed. McGraw-Hill International Edition, Singapore.

[17] Shigley, J.E. & Mischke, C.R. (1989). Mechanical Designers Workbook: Corrosion and wear, McGraw-Hill Company, New York

[18] Sadek, S. & Olsson, M. (2014). New models for prediction of high cycle fatigue failure based on highly loaded regions, *International Journal of Fatigue*, 66, 101-110.

[19] Ihueze, C.C., Okafor, C.E.& Okoye, C.I. (2013). Natural Fibers Composites Design and Characterization for Limit Stress Prediction in Multiaxial Stress State, *Journal of King Saud University - Engineering Sciences*, Elsevier, doi: http://dx.doi.org 10.1016/j.jksues.2013.08.002

[20] Gross, A.J. & Ravi-Chandar, K .(2014). Prediction of ductile failure using a local strain-to-failure criterion, *International Journal of Fracture*,186, 66-91, DOI 10.1007/s10704-013-9908-2.

[21] Mohotti, D., Ali, M., Ngo, T., Lu, J. & Mendis, P. (2014). Strain rate dependent constitutive model for predicting material behaviour of polyurea under high strain rate tensile loading, Materials and Design, 53, 830-837. DOI:10.1016/j.matdes.2013.07.020

[22] Ihueze, C.C. & Mgbemena C.O. (2014). Modeling Hyperelastic Behavior of Natural Rubber/Organomodified Kaolin Composites Oleochemically Derived from Tea Seed Oils (*Camellia sinensis*) for Automobile Tire Side Walls Application, *Journal of Scientific Research Reports*, 3(19), 2538-2551.

[23] Mgbemena, C.O, Ibekwe., N.O., Rugmini. S., Menon, & A.R.R. (2013a). Characterization of kaolin intercalates of oleochemicals derived from rubber seed (Hevea brasiliensis) and tea seed (Camelia sinensis) oils, Journal of King Saud University - Science, Volume 25, Issue 2,Pages 149-155.

[24] Mgbemena, C.O., Ibekwe, N.O., Mohamed, A., Rugmini. S., & Menon, A.R.R. (2013b).Thermal Behavior and UV Properties of Organomodified Kaolin Oleochemically Derived from Rubber Seed Oils (Hevea brasiliensis) and Tea Seed Oils (Camellia sinensis), Journal of Surface Engineered Materials and Advanced Technology, Vol. 3 No. 3, pp. 163-168. doi: 10.4236/jsemat.2013.33021.

[25] Rugmini, S., & Menon, A. R. R. 2008. Organomodified Kaolin as Filler for Natural Rubber, Journal of Applied Polymer Science, 107, pp. 3476-3483.

[26] Crawford, R.J. (1998). Plastic Engineering, 3rd edition, Butterworth-Heinamann, Oxford Maiti, M.,& Bhowmick, A.K. (2006). New insights into rubber-clay composites by AFM imaging, *Polymer*, 47, 6156-6166.